

# Rational Stabilization of Helix 2 of the Prion Protein Prevents Its Misfolding and Oligomerization

Jogender Singh, Harish Kumar, Ambadi T. Sabareesan, and Jayant B. Udgaonkar\*

National Centre for Biological Sciences, Tata Institute of Fundamental Research, Bengaluru 560065, India

**S** Supporting Information

**ABSTRACT:** Designed stabilization of helix 2 of the mouse prion protein is shown to lead to an increase in global stability of the protein. Studies of hydrogen exchange coupled to mass spectrometry confirm that the increase in stability is confined primarily to helix 2, and that it accounts for the global stabilization of the protein. Importantly, such localized stabilization of the protein can completely inhibit its ability to form oligomers and slows down amyloid fibril formation.

Prion diseases are fatal neurodegenerative diseases, caused by the misfolding of monomeric, mostly  $\alpha$ -helical cellular prion protein (PrP<sup>C</sup>) into multimeric, mostly  $\beta$ -rich PrP<sup>Sc</sup>.<sup>1</sup> While accumulation of PrP<sup>Sc</sup> in the central nervous system is characteristic of prion diseases, the mechanisms of misfolded PrP toxicity are yet to be fully understood. Misfolded PrP is found in fibrillar as well as in soluble oligomeric forms, and both the former<sup>2a,b</sup> and latter<sup>2b-d</sup> forms have been shown to be toxic, *in vitro* and *in vivo*. In all cases, aggregation of PrP is linked to its misfolding. Clearly, understanding the structural basis of the misfolding of PrP is important for understanding prion pathogenesis.<sup>3</sup>

Recombinant prion protein can be converted into either amyloid fibrils or soluble oligomers *in vitro* under different environmental conditions.<sup>4</sup> Amyloid fibrils are typically generated at physiological pH in the presence of denaturants and upon physical shaking,<sup>4</sup> and appear to form directly from monomeric protein.<sup>5</sup> On the other hand, soluble,  $\beta$ -rich oligomers are seen to form at low pH,<sup>4,6</sup> and have been shown to be cytotoxic.<sup>2b,c</sup> Importantly, sporadic prion disease susceptibility appears to correlate well with the propensity of recombinant PrP to form  $\beta$ -rich oligomers *in vitro* at low pH,<sup>7</sup> and such oligomers have been shown to be adept at disrupting lipid membranes.<sup>8</sup> But the molecular details of the conversion of monomeric PrP into misfolded oligomeric and fibrillar forms are poorly understood.

In some models proposed for the structure of PrP aggregates, helical structure is retained,<sup>3</sup> but recent experimental studies on recombinant PrP fibrillar aggregates generated under different environmental conditions suggest that helices 2 ( $\alpha 2$ ) and 3 ( $\alpha 3$ ) have converted into  $\beta$ -sheet, whether probed by EPR,<sup>9</sup> hydrogen–deuterium exchange (HDX),<sup>5,8</sup> solution NMR,<sup>10</sup> or solid-state NMR.<sup>11</sup> In brain-derived fibrils of PrP too, major conformational rearrangements in  $\alpha 2$  and  $\alpha 3$ <sup>12</sup> appear to have taken place. HDX studies on  $\beta$ -rich oligomers formed *in vitro* at low pH,<sup>8</sup> indicate that  $\alpha 2$  and  $\alpha 3$  have undergone large structural

changes in the oligomers, similar in pattern to those seen in HDX studies on fibrils,<sup>3,8</sup> except that the converted structures in the oligomers are not as stable (to HDX) as those in fibrils. In the case of moPrP fibrils,  $\alpha 2$  and  $\alpha 3$  have been shown to undergo structural transformation early during recombinant PrP aggregation,<sup>5,13</sup> suggesting that the information regarding conformational conversion is resident in either or both of  $\alpha 2$  and  $\alpha 3$ .

$\alpha 2$  of mammalian PrPs is very unusual in its amino acid composition, with several amino acid residues, especially the sequence stretch TVTTTT (residues 187–192, mouse numbering) at its C-terminus (Supporting Information (SI) Figure S1), having a high propensity for  $\beta$ -sheet formation.<sup>14</sup> Importantly, the TVTTTT stretch is highly conserved in the PrPs of mammals that can be infected with prion disease, and it is absent in non-mammalian PrPs which do not aggregate and cause prion disease.<sup>14</sup> The C-terminus of  $\alpha 2$  is also the region that exhibits the most structural perturbation upon a reduction in pH, and in the presence of chemical denaturants.<sup>15</sup> Hence, the C-terminus of  $\alpha 2$  is likely to play an early role in effecting conformational change during the formation of PrP oligomers under various conditions, but this role has not been delineated.

To probe the role of the C-terminus of  $\alpha 2$  of recombinant mouse prion protein (moPrP) in effecting misfolding and oligomerization, the amino acid residues in the sequence stretch TVTTTT were replaced either completely or partly (see below) with alanine, which has the highest propensity for  $\alpha$ -helix formation.<sup>16</sup> Four different recombinant mutant proteins were generated. In the first variant (A6 moPrP), TVTTTT was replaced with AAAAAA. In the second variant (A4 moPrP), TTTT, a very unusual sequence stretch for a helix,<sup>14</sup> was replaced with AAAA. In the third variant (A3\* moPrP), the three least surface-exposed residues in TVTTTT were replaced with alanine to yield the sequence stretch AVTAAT. In the fourth variant (A3 moPrP), the three most surface-exposed residues in TVTTTT were replaced with alanine to yield the sequence stretch TAATTA (Figure S1). The identity and purity of each of the four mutant proteins were confirmed by mass spectrometry (MS) (data not shown). At pH 4, the four mutant proteins show native-state circular dichroism (CD) spectra very similar to that of wt moPrP (data not shown) indicating that no change in the secondary structure (Figure S1) has taken place because of the mutations.

Received: August 1, 2014

Revised: October 24, 2014

Published: November 19, 2014

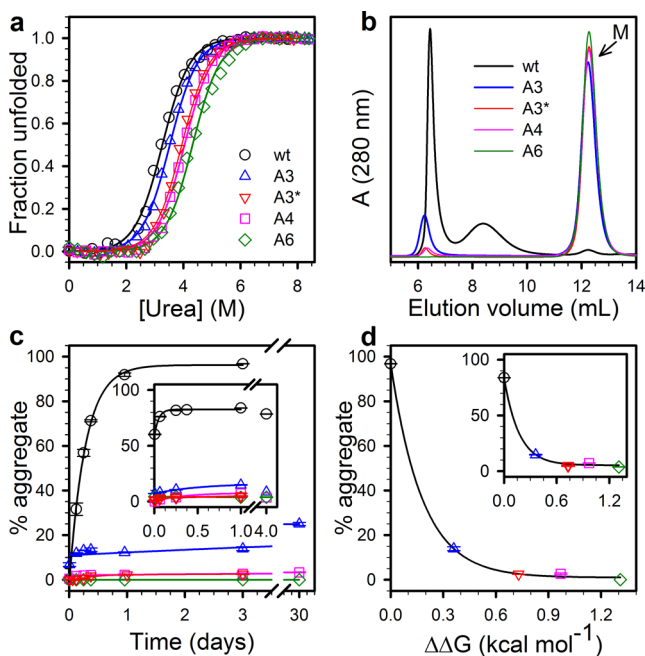


**Figure 1.** Effect of mutations on the stability and misfolding of moPrP. (a) Urea-induced equilibrium unfolding transitions of wt, A3, A3\*, A4, and A6 moPrP at pH 4, 25 °C as monitored by far-UV CD at 222 nm. (b) SEC of the different moPrP variants at 3 days of incubation of 100 μM protein in 150 mM NaCl buffer at 37 °C, pH 4. “M” indicates the monomer peak. (c) Percent aggregate formed at different times of aggregation of the different moPrP variants at 100 μM concentration in 150 mM NaCl, 1 M GdnHCl, and 3 M urea at 37 °C, pH 4. Inset: percent aggregate formed at different times of aggregation of the different moPrP variants at 100 μM concentration in 150 mM NaCl, 1 M GdnHCl, and 3 M urea at 37 °C, pH 4. (d) Percent aggregate formed at 3 days by the different moPrP variants at 100 μM concentration in 150 mM NaCl at 37 °C, pH 4, is plotted against the increase in stability ( $\Delta\Delta G$ ) over that of wt moPrP. Inset: percent aggregate formed vs  $\Delta\Delta G$  at 24 h of reaction of 100 μM protein in 150 mM NaCl, 1 M GdnHCl, 3 M urea at 37 °C, pH 4. The symbols and colors are the same for the different moPrP variants in all panels. See Table S1 for the  $\Delta\Delta G$  values for the different moPrP variants. The continuous lines through the data points in (c) and (d) were drawn by inspection to guide the eye. Error bars represent the spread in data from two independent experiments.

Denaturant-induced equilibrium unfolding transitions of A3, A3\*, A4, and A6 moPrP, under conditions where moPrP is monomeric (SI text), show that they are significantly more stabilized than the wt protein, at pH 4 (Figure 1a) and at pH 7 (Figure S2a), and that the stability increases in the order wt < A3 < A3\* < A4 < A6 moPrP (Tables S1 and S2). The midpoints ( $T_m$ ) of thermally induced unfolding transitions at pH 4 also increase in the same order (Figure S2b) with the increase in  $T_m$  being quite large ( $\Delta T_m \approx 10$  °C) for A4 and A6 moPrP. Since it is known that the disulfide bond in PrP is important for its conformational stability,<sup>17</sup> it was important to establish that the observed differences in stability between the different moPrP variants are not because of the disulfide bond having become reduced for some of the protein variants during measurement. This was done by checking whether the denaturant-unfolded proteins are amenable to labeling by the thiol reagent DTNB; they were found not to be so (Figure S3 and SI text). Hence, the increase in the stabilities of the mutant proteins is not because of differences in their oxidation status. The data (Tables S1 and S2) indicate that all six residues in the TVT<sup>106</sup>TTT sequence stretch are involved in destabilizing the wt protein.

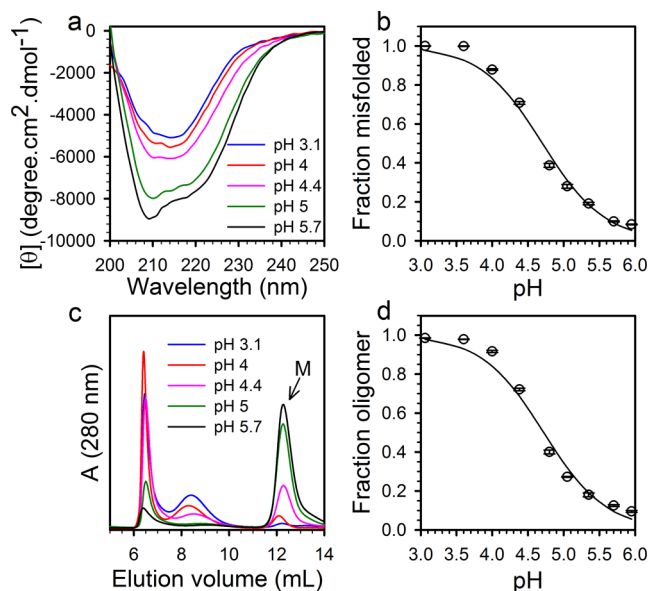


**Figure 2.** pH dependence of misfolding and oligomerization of wt moPrP. (a) Far-UV CD spectra of wt moPrP at 24 h of oligomerization in the presence of 150 mM NaCl, at 37 °C and at various pH values. (b) Fraction misfolded form at 24 h vs pH. The fraction misfolded form was calculated by using the fractional change in CD signal at 216 nm. (c) SEC profiles of wt moPrP at 24 h of oligomerization in the presence of 150 mM NaCl, at 37 °C and at various pH values. “M” indicates the monomer peak. (d) Percent oligomer formed at 24 h vs pH. The lines through the data points in (b) and (d) represent fits to eq S1 (SI). Both fits yield an apparent  $pK_a = 4.7$  for misfolding and oligomer formation. Error bars represent the spread in data from two independent experiments.

PrP is known to misfold and form oligomers at low pH in the presence of added salt.<sup>6,15b</sup> Misfolding, as monitored by the change in CD signal at 216 nm, is linked to oligomer formation, as monitored by size-exclusion chromatography (SEC), by recombinant moPrP (Figure 2a,c) at low pH in the presence of 150 mM NaCl at 37 °C and requires the protonation of a yet unidentified amino acid residue with an apparent  $pK_a = 4.7$  (Figure 2b,d and SI text). Quite clearly, wt moPrP misfolds and forms oligomers at pH values that the protein is exposed to *in vivo*. In cells, aggregation of PrP has been shown to occur in the endocytic pathway,<sup>18</sup> and at the pH prevalent in late endosomes/lysosomes (pH ~5), ~30% of the protein would be misfolded and oligomeric, while at the pH present at the cell surface (pH ~7), <1% of the protein would be protonated and thereby misfolded into oligomeric form. Hence, misfolding and oligomer formation are not detectable at pH 7. *In vitro*, it then becomes convenient to study oligomer formation at a lower pH where the concentration of the oligomerization-competent, critically protonated state is high and, consequently, both the extent and kinetics of oligomer formation are easily measurable.

The observation that >95% of the protein is present in oligomers at pH 4 is important, because sporadic prion disease susceptibility in different mammals has been shown to be directly correlated with the extent to which moPrP oligomerizes at this pH.<sup>7</sup> Moreover, the oligomers formed at pH 4 make lipid membrane permeable to a large solute, PEG, 1 kDa in molecular weight (Figure S4 and SI text). The ability of the oligomers to disrupt membrane structure at pH 4, as they do at pH 2,<sup>8</sup> points to a mechanism by which they may be toxic to cells. It has been speculated that one explanation for why prion diseases are late-

onset diseases may be that the concentration of the aggregation-competent critically protonated state is extremely small at physiological pH and, consequently, aggregation is very slow.<sup>19</sup>

Since more than 95% of wt moPrP forms oligomers at 100  $\mu$ M concentration, in the presence of 150 mM NaCl, at pH 4 and at 37  $^{\circ}$ C, the effect of the increase in the stability of moPrP on its oligomerization under these conditions was studied using SEC (Figure 1b). For A3, A3\*, A4, and wt moPrP, the equilibrium between monomer and oligomer is reached within 3 days, after which the amount of oligomer does not change up to 30 days (Figure 1c). The amount of oligomer formed is found to decrease in the order wt > A3 > A3\*  $\approx$  A4 moPrP (Figure 1c). AFM imaging showed spherical oligomer formation for wt moPrP, and slightly elongated oligomers for A3, A3\*, and A4 moPrP, and the amount of oligomers decrease in the order wt > A3 > A3\*  $\approx$  A4 moPrP (Figure S5a). Remarkably, A6 moPrP does not show any oligomer formation even after 30 days (Figure 1c).

It was important to determine whether A6 moPrP could be induced to oligomerize under other conditions that facilitate the oligomerization of wt moPrP. In the presence of both 1 M guanidine hydrochloride (GdnHCl) and 3 M urea,<sup>4</sup> the rate of oligomer formation is faster than, but the extent of final oligomerization is the same as, when the denaturants are absent (Figure 1c, inset) for each of the mutant and wt proteins (Figure S6). Remarkably, A6 moPrP does not show any oligomer formation even after 4 days in the presence of the denaturants, whereas wt moPrP has fully oligomerized at 6 h. Similarly, at pH 2 in the presence of 150 mM NaCl at 25  $^{\circ}$ C, and at 100  $\mu$ M moPrP concentration, the rate of aggregate formation is much faster than at pH 4. But whereas wt moPrP oligomerizes fully within 1 h at pH 2, A6 moPrP does not form any oligomer, even at 10 h (Figure S7a). Indeed, A6 moPrP retains its complete native secondary structure (Figure S7b), as detected by CD. Surprisingly, the A3, A3\*, and A4 moPrP oligomers formed at pH 2 were found to have proceeded to form worm-like amyloid fibrils (Figure S5b) at 1 h of aggregation, whereas wt moPrP oligomers take  $\sim$ 100 h to do so.<sup>6</sup>

The amount of oligomer formed at pH 4, both in the absence (Figure 1d) and presence of added denaturants (Figure 1d inset), shows an exponential decrease with increasing protein stability, indicating that even minor stabilization of moPrP leads to a relatively large decrease in its oligomerization. Far-UV CD spectra showed that the oligomer formed at different times is  $\beta$ -rich, while the monomer is  $\alpha$ -helical, as can be seen for A3\*, A4, and A6 moPrP (Figure S8).

The extent of misfolded aggregate formation decreases with increasing global stability of moPrP, and it was important to determine how it is affected by the local stability and dynamics of  $\alpha$ 2, and whether the mutations specifically stabilize  $\alpha$ 2. To this end, HDX coupled with MS was used to probe the structural dynamics in different secondary structural regions. In HDX-MS studies, the amide hydrogen sites that are protected against HDX can be localized to specific segments of the protein sequence by MS analysis of peptides generated from the protein by proteolytic digestion at low pH, after the HDX reaction is complete. A peptide map generated earlier<sup>8</sup> was used for the current study. HDX into the native protein was carried out at pH 4, because this pH is close to the pH at which intrinsic HDX rates are at their minimum. This allows observation of HDX at the maximum number of amide hydrogen sites, spread over all the secondary structural elements of the protein structure.

The kinetics of deuterium incorporation into each of the different secondary structural regions are very similar for wt, A3,

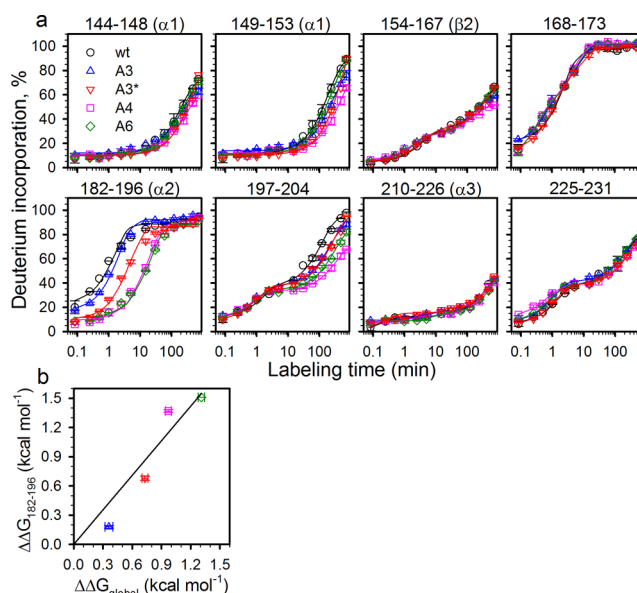


**Figure 3.** Time course of labeling by HDX of different secondary structure regions of moPrP variants at pH 4. (a) Percent deuterium incorporation profiles of selected sequence segments of wt (black circle), A3 (blue triangle), A3\* (red inverted triangle), A4 (purple square), and A6 (green diamond) moPrP at 25  $^{\circ}$ C, pH 4. Error bars represent the spread in data from two independent experiments. The lines through the data represent the fits to either a monoexponential or a biexponential curve. (b) Comparison of the  $\Delta\Delta G_{182-196}$  (kcal mol $^{-1}$ ) calculated from HDX labeling rates, with the global  $\Delta\Delta G$ .

A3\*, A4, and A6 moPrP, and differ for the five proteins only for the labeling of  $\alpha$ 2 (Figures 3a and S9). The sequence segment 182–196 covering the C-terminus of  $\alpha$ 2, shows higher protection against deuterium labeling for A3, A3\*, A4, and A6 moPrP than for wt moPrP. A slight increase in protection against deuterium labeling was also observed for the segment 197–204, most likely because stabilization of the C-terminus of  $\alpha$ 2 might render this spatially adjacent region conformationally less flexible.

wt moPrP has been shown to form both large and small oligomers at low pH, with the former shown to be on-pathway and the latter shown to be off-pathway, to worm-like fibril formation at pH 2.<sup>19</sup> Interestingly, A3, A3\*, and A4 moPrP, unlike wt moPrP, are seen to form elongated oligomers and worm-like fibrils at pH 4 and pH 2, respectively, while A6 moPrP does not form any aggregate (Figure S5). One difference in the structures of the large and small oligomers and the worm-like fibrils formed by wt moPrP is that the sequence stretch 190–197 is more protected against HDX in the small oligomer than in the large oligomer and the worm-like fibrils.<sup>8</sup> Moreover, the 190–197 stretch is as unprotected in the large oligomer and the worm-like fibrils as it is in the monomer. It appears that the 190–197 sequence stretch, which is nearly completely helical in the monomer, acquires non-native structure in the small oligomer formed by wt moPrP, and that the small oligomer cannot form from the monomer when this region is stabilized upon mutation because this critical non-native structure cannot then form. Partial stabilization of this stretch of amino acids in A3, A3\*, and A4 moPrP might also be responsible for rapid formation of the worm-like fibrils by A3, A3\*, and A4 moPrP. Nevertheless, the fraction of monomer that does not aggregate increases in the order wt < A3 < A3\* < A4 < A6 moPrP, while A6 moPrP does not show any aggregate formation at pH 2 or pH 4.

The HDX rates were used to calculate the thermodynamic stability of segment 182–196 (see SI). Importantly, the local thermodynamic stability in this region increases in the order: A3 < A3\* < A4 < A6 moPrP. More importantly, the local  $\Delta\Delta G$  values for segment 182–196 correlate very well with the global  $\Delta\Delta G$  values (Figure 3b): a plot of local  $\Delta\Delta G$  vs global  $\Delta\Delta G$  has a slope of 1.20. It appears that the increase in the global thermodynamic stability of the mutant variants of moPrP can be accounted for predominantly by the increase in the stability of  $\alpha 2$ , and that the mutations in the C-terminus of  $\alpha 2$  do not significantly affect other secondary structure regions of the protein.

The correlations observed between local stabilization of  $\alpha 2$  and global stabilization (Figure 3b), and between stabilization and the extent of oligomer formation (Figure 1d), are seen for mutations that alter the entire TVTTTT sequence stretch (A6 moPrP), a full helical turn, (A4 moPrP), or only solvent-exposed residues (A3 moPrP). The correlations suggest that the local stabilization of the C-terminus of  $\alpha 2$  is responsible for decreased oligomer formation by the mutant proteins. In A3\* moPrP, only those residues in the TVTTTT sequence stretch not solvent-exposed were mutated to Ala. The observation that A3\* moPrP does not violate these correlations, makes it unlikely that the decreased extent of oligomerization is because the mutations perturb the surface at the C-terminus of  $\alpha 2$  in a manner that prevents the protein–protein interactions that drive oligomerization. It should be noted that the TVTTTT sequence stretch is conserved among all mammals that can be infected with prion disease,<sup>20</sup> making it very unlikely that it determines the species barrier to prion infection.

Interestingly, all the mutant proteins form long straight amyloid fibrils at pH 7 in the presence of 2 M GdnHCl and upon physical agitation (Figure S10 and SI text). The initial lag phase seen in the kinetics of fibril formation at pH 7 increases in the order wt < A3  $\approx$  A3\* < A4 < A6 moPrP (Figure S11a,b) and is correlated with the increasing stability of the moPrP variants (Figure S11c).

Stabilization of the native structure of a protein is known to disfavor its aggregation,<sup>21</sup> but it is not straightforward to do this in a predictable manner by protein engineering. The current study made use of previous observations suggesting that the C-terminus of  $\alpha 2$  is susceptible to local unfolding,<sup>15</sup> and might thus be important in the initiation of PrP misfolding. It is quite remarkable that rational and specific stabilization of the C-terminus of  $\alpha 2$  can completely abolish PrP misfolding and oligomerization at low pH, as has now been shown. The current study provides a rationale for the observation that several anti-prion drugs, which were proven to be effective in *ex vivo* and *in vivo* experiments, bind specifically to the C-terminus of  $\alpha 2$ :<sup>22</sup> the drug binding must lead to local stabilization of  $\alpha 2$ , thereby preventing the initiation of oligomer formation.

## ■ ASSOCIATED CONTENT

### ● Supporting Information

Experimental details, and supplementary figures and tables. This material is available free of charge via the Internet at <http://pubs.acs.org>.

## ■ AUTHOR INFORMATION

### Corresponding Author

[jayant@ncbs.res.in](mailto:jayant@ncbs.res.in)

### Notes

The authors declare no competing financial interest.

## ■ ACKNOWLEDGMENTS

We thank members of our laboratory, as well as M. K. Mathew and S. Gosavi, for discussion and for their comments on the manuscript. We thank Nivin Mothi for help in carrying out fibril formation assays at pH 7. The AFM images were collected at the Central Imaging Facility of the National Centre for Biological Sciences. J.B.U. is a recipient of a J.C. Bose National Fellowship from the Government of India. This work was funded by the Tata Institute of Fundamental Research and by the Department of Biotechnology, Government of India.

## ■ REFERENCES

- (1) Prusiner, S. B. *Science* **1997**, *278*, 245.
- (2) (a) Novitskaya, V.; Bocharova, O. V.; Bronstein, I.; Baskakov, I. V. *J. Biol. Chem.* **2006**, *281*, 13828. (b) Sanghera, N.; Wall, M.; Vénien-Bryan, C.; Pinheiro, T. J. *Biochim. Biophys. Acta* **2008**, *1784*, 873. (c) Kristiansen, M.; Deriziotis, P.; Dimcheff, D. E.; Jackson, G. S.; Ova, H.; Naumann, H.; Clarke, A. R.; van Leeuwen, F. W.; Menéndez-Benito, V.; Dantuma, N. P.; Portis, J. L.; Collinge, J.; Tabrizi, S. J. *Mol. Cell* **2007**, *26*, 175. (d) Simoneau, S.; Rezaei, H.; Salès, N.; Kaiser-Schulz, G.; Lefebvre-Roque, M.; Vidal, C.; Fournier, J. G.; Comte, J.; Wopfner, F.; Grosclaude, J.; Schätzl, H.; Lasmézas, C. I. *PLoS Pathog.* **2007**, *3*, No. e125.
- (3) Diaz-Espinoza, R.; Soto, C. *Nat. Struct. Mol. Biol.* **2012**, *19*, 370.
- (4) Baskakov, I. V.; Legname, G.; Baldwin, M. A.; Prusiner, S. B.; Cohen, F. E. *J. Biol. Chem.* **2002**, *277*, 21140.
- (5) Singh, J.; Udgaonkar, J. B. *J. Mol. Biol.* **2013**, *425*, 3510.
- (6) Jain, S.; Udgaonkar, J. B. *J. Mol. Biol.* **2008**, *382*, 1228.
- (7) Khan, M. Q.; Sweeting, B.; Mulligan, V. K.; Arslan, P. E.; Cashman, N. R.; Pai, E. F.; Chakrabarty, A. *Proc. Natl. Acad. Sci. U.S.A.* **2010**, *107*, 19808.
- (8) Singh, J.; Sabareesan, A. T.; Mathew, M. K.; Udgaonkar, J. B. *J. Mol. Biol.* **2012**, *423*, 217.
- (9) Cobb, N. J.; Apetri, A. C.; Surewicz, W. K. *J. Biol. Chem.* **2008**, *283*, 34704.
- (10) Schlepckow, K.; Schwalbe, H. *Angew. Chem., Int. Ed.* **2013**, *52*, 10002.
- (11) Tycko, R.; Savtchenko, R.; Ostapchenko, V. G.; Makarava, N.; Baskakov, I. V. *Biochemistry* **2010**, *49*, 9488.
- (12) (a) Gong, B.; Ramos, A.; Vázquez-Fernández, E.; Silva, C. J.; Alonso, J.; Liu, Z.; Requena, J. R. *Biochemistry* **2011**, *50*, 4963. (b) Smirnovas, V.; Baron, G. S.; Offerdahl, D. K.; Raymond, G. J.; Caughey, B.; Surewicz, W. K. *Nat. Struct. Mol. Biol.* **2011**, *18*, 504.
- (13) Chen, J.; Thirumalai, D. *Biochemistry* **2013**, *52*, 310.
- (14) Dima, R. I.; Thirumalai, D. *Biophys. J.* **2002**, *83*, 1268.
- (15) (a) Hosszu, L. L.; Wells, M. A.; Jackson, G. S.; Jones, S.; Batchelor, M.; Clarke, A. R.; Craven, C. J.; Waltho, J. P.; Collinge, J. *Biochemistry* **2005**, *44*, 16649. (b) Bjorndahl, T. C.; Zhou, G. P.; Liu, X.; Perez-Pineiro, R.; Semenchenko, V.; Saleem, F.; Acharya, S.; Bujold, A.; Sobsey, C. A.; Wishart, D. S. *Biochemistry* **2011**, *50*, 1162.
- (16) Blaber, M.; Zhang, X. J.; Matthews, B. W. *Science* **1993**, *260*, 1637.
- (17) Maiti, N. R.; Surewicz, W. K. *J. Biol. Chem.* **2001**, *276*, 2427.
- (18) Arnold, J. E.; Tipler, C.; Laszlo, L.; Hope, J.; Landon, M.; Mayer, R. J. *J. Pathol.* **1995**, *176*, 403.
- (19) Jain, S.; Udgaonkar, J. B. *Biochemistry* **2011**, *50*, 1153.
- (20) van Rheede, T.; Smolenaars, M. M.; Madsen, O.; de Jong, W. W. *Mol. Biol. Evol.* **2003**, *20*, 111.
- (21) (a) Chiti, F.; Taddei, N.; Bucciantini, M.; White, P.; Ramponi, G.; Dobson, C. M. *EMBO J.* **2000**, *19*, 1441. (b) Hammarström, P.; Schneider, F.; Kelly, J. W. *Science* **2001**, *293*, 2459. (c) Kong, Q.; Mills, J. L.; Kundu, B.; Li, X.; Qing, L.; Surewicz, K.; Cali, I.; Huang, S.; Zheng, M.; Swietnicki, W.; Sönnichsen, F. D.; Gambetti, P.; Surewicz, W. K. *Cell Rep.* **2013**, *4*, 248.
- (22) Kamatari, Y. O.; Hayano, Y.; Yamaguchi, K. I.; Hosokawa-Muto, J.; Kuwata, K. *Protein Sci.* **2013**, *22*, 22.